Received 28 May 2023; revised 22 June 2023; accepted 2 July 2023. Date of publication 5 July 2023; date of current version 27 July 2023.

Digital Object Identifier 10.1109/OJCOMS.2023.3292521

SSK-Based PSK-LoRa Modulation for IoT Communications

QUANTAO YU [1], DONGXUAN HE [1], ZHIPING LU [2,3], AND HUA WANG [1] (Member, IEEE)

[1]School of Information and Electronics, Beijing Institute of Technology, Beijing 100081, China

[2]School of Information and Communication Engineering, Beijing University of Posts and Telecommunications, Beijing 100876, China

[3]State Key Laboratory of Wireless Mobile Communications, China Academy of Telecommunications Technology, Beijing 100191, China

CORRESPONDING AUTHORS: D. HE and Z. LU (e-mail: dongxuan_he@bit.edu.cn; luzp@cict.com)

This work was supported in part by the National Key Research and Development Program of China under Grant 2020YFB1807900; in part by the State Key Laboratory of Wireless Mobile Communications, China Academy of Telecommunications Technology under Grant CATT.KX.2023.161; and in part by the National Natural Science Foundation of China under Grant 62101306.

ABSTRACT LoRa has been considered as a key enabler for the next generation Internet of Things (IoT) networks. However, the low spectral efficiency (SE) of chirp spread spectrum (CSS) modulation used in LoRa is a fatal drawback for its extensive applications in the sixth generation (6G) enabled high-data-rate IoT era. In this paper, we propose SSK PSK-LoRa (slope-shift-keying and phase-shift-keying LoRa) modulation, which can achieve higher SE and better energy efficiency (EE) than the conventional LoRa modulation. In particular, the transceiver architecture of our proposed scheme is presented along with both coherent and semi-coherent detection methods. Moreover, the orthogonality of SSK PSK-LoRa symbols is analyzed and the closed-form approximations for bit error rate (BER) in both additive white Gaussian noise (AWGN) and Rayleigh fading channels are derived. Numerical results demonstrate the superiority of our proposed modulation scheme, which outperforms most classical counterparts in terms of BER and effective throughput.

INDEX TERMS Internet of Things (IoT), LoRa, chirp spread spectrum (CSS), waveform design.

I. INTRODUCTION

THE SIXTH generation (6G) wireless network is envisioned to realize a revolution of fully intelligent and autonomous society via the Internet of Things (IoT) [1]. It aims to provide seamless connectivity not only to humans but also to machine type devices [2]. In general, IoT applications can be classified into four categories: massive IoT, broadband IoT, critical IoT, and industrial automation IoT [3]. Specifically, the massive IoT requires data collection where a massive number of low-cost devices sporadically transmit small volume of data to the cloud [4]. In particular, a multitude of applications characterized by low power and long range communications, such as smart city, smart agriculture, asset tracking, etc., have driven the emergence and proliferation of LPWAN (low power wide area network) technologies [5], [6]. Among the state-of-the-art LPWAN technologies, LoRa has attracted widespread interest from both academia and industry as it provides an impeccable infrastructure for massive IoT [7], [8]. As a result, an efficient integration of LoRa into 6G network is desirable [9], [10].

From the technical perspective, LoRa can be categorized into two layers: physical (PHY) layer using chirp spread spectrum (CSS) modulation (i.e., LoRa modulation) and medium access control (MAC) layer with ALOHA-based protocol (i.e., LoRaWAN protocol). For LoRa modulation, a set of orthogonal chirp signals (i.e., upchirps) are used to represent the modulation symbols, where the information bearing elements are the initial frequency shifts (FSs) of the modulated upchirps. Several recent studies have presented a detailed mathematical description of LoRa modulation. Specifically, Vangelista gave a digital signal processing description of LoRa modulation and provided a theoretical derivation of the optimum receiver based on discrete Fourier transform (DFT) [11]. Moreover, the authors in [12] provided a complete characterization of LoRa signal model, which includes both the analytical expression of LoRa signal in the

This work is licensed under a Creative Commons Attribution 4.0 License. For more information, see https://creativecommons.org/licenses/by/4.0/

TABLE 1. Comparisons of different multi-parameter CSS modulation schemes.

Modulation	Information Bearing Elements
E-LoRa [21]	Initial FS of single modulated chirp with initial PS 0 or $\pi/2$
PSK-LoRa [19], [20]	Initial FS and initial PS of single modulated chirp
ePSK-LoRa [22]	Initial FSs and initial PSs of multiple modulated chirps
SSK-LoRa [23]	Initial FS of single modulated chirp with either upchirp or downchirp
DCRK-CSS [24]	Initial FS and chirp rate of single modulated chirp

time domain and closed-form expressions of its continuous and discrete spectra. Based on the mathematical descriptions of LoRa modulation, Elshabrawy and Robert [13] derived the closed-form approximations for the underlying bit error rate (BER) of LoRa modulation in both additive white Gaussian noise (AWGN) and Rayleigh fading channels. Benefited from the processing gain of CSS modulation, the transmitted information can be recovered even when the received signal-to-noise ratio (SNR) is negative, making it a promising candidate for low power and long range IoT communications. However, the high energy efficiency (EE) of LoRa modulation is achieved at the cost of low spectral efficiency (SE) and data rate, which has become a bottleneck for its extensive applications. Specifically, it has been confirmed that the maximum achievable data rate of LoRa modulation is only 27 kbps [14], which limits many practical applications such as smart building [15], image transmission [16], and industrial IoT [17], [18]. Therefore, some researchers have proposed alternative CSS-based modulation schemes, which show higher spectral and/or energy efficiency than the conventional LoRa modulation.

To improve the SE, one feasible way is to convey additional information bits by exploiting other chirp signal parameters, which can be characterized as multi-parameter CSS modulation. In general, there are four different parameters that can be utilized to encode the information bits, including amplitude, chirp rate, initial FS, and initial phase shift (PS). For example, Nguyen et al. [19] and Bomfin et al. [20] proposed phase shift keying LoRa (PSK-LoRa) modulation, which embeds extra information bits in the initial PS. Notably, the so called extended LoRa (E-LoRa) modulation can be regarded as a special variant of BPSK-LoRa modulation [21]. Furthermore, the authors in [22] proposed an enhanced PSK-LoRa (ePSK-LoRa) modulation, which is capable of achieving higher SE and better EE than PSK-LoRa at the cost of higher peak-to-average-power ratio (PAPR) and computational complexity. In addition, encoding additional information bits in the chirp rate has been proposed in [23], [24], named slope-shift-keying LoRa (SSK-LoRa) modulation and discrete chirp rate keying CSS (DCRK-CSS) modulation. Specifically, two discrete chirp rates (i.e., upchirps and downchirps) are utilized in SSK-LoRa modulation to convey one more information bit within each modulation symbol. As an extension of SSK-LoRa modulation, multiple discrete chirp rates are used in DCRK-CSS modulation to convey more additional information bits. The characteristics of these multi-parameter CSS modulation schemes are summarized in Table 1.

Motivated by the above research, a novel SSK PSK-LoRa modulation is proposed in this work, which can further improve the SE and data rate. The main contributions of this paper are summarized as follows.

1) We propose a new multi-parameter CSS modulation scheme, namely SSK PSK-LoRa modulation, and present its transceiver architecture as well as coherent and semi-coherent detection methods.
2) The orthogonality of SSK PSK-LoRa symbols is analyzed. Moreover, with the help of interference analysis, the closed-form approximations for BER of semi-coherent detection in both AWGN and Rayleigh fading channels are derived.
3) Performance comparison of the proposed scheme and other CSS-based modulation schemes is provided. Both analytical and numerical results are presented to demonstrate the superiority of our proposed scheme in terms of both EE and SE.

The rest of this paper is organized as follows. Section II presents the system model of our proposed SSK PSK-LoRa modulation, including its transmission and detection. Section III elucidates the orthogonality of SSK PSK-LoRa symbols and analyzes the interference at the receiver. Section IV derives the closed-form approximations for BER of the proposed scheme in both AWGN and Rayleigh fading channels. Numerical results and discussions are presented in Section V. Finally, Section VI concludes the whole paper.

II. SYSTEM MODEL

A. BASIC DEFINITIONS

The basic definitions of some main parameters throughout this paper are presented here.

- B is the occupied bandwidth of LoRa radio signals, which is typically set to be 125, 250, or 500 kHz.

Without loss of generality, we set $B = 125$ kHz in this paper.

- SF is the spreading factor ranging from 7 to 12, which determines the processing gain of LoRa modulation and denotes the number of information bits within each LoRa symbol.
- N_F represents the number of information bits encoded in the FS of the transmitted chirp.
- N_P represents the number of information bits encoded in the PS of the transmitted chirp.
- N_C represents the number of information bits encoded in the chirp rate of the transmitted chirp.

In the complex baseband-equivalent form, each chirp can be defined by $M = 2^{SF}$ samples. We denote the basic upchirp and basic downchirp as $u[n]$ and $d[n]$, respectively, given by

$$u[n] = \frac{1}{\sqrt{M}} \exp\left\{j\frac{\pi n^2}{M}\right\}, \tag{1}$$

$$d[n] = \frac{1}{\sqrt{M}} \exp\left\{-j\frac{\pi n^2}{M}\right\}, \tag{2}$$

where $n = 0, 1, \ldots, M-1$ is the sample index.

B. TRANSMISSION

In the conventional PSK-LoRa modulation, M orthogonal upchirps are used to represent the modulation symbols. The transmitted signal, denoted by $x[n]$, is given as

$$\begin{aligned} x[n] &= \frac{1}{\sqrt{M}} \exp\left\{j\frac{\pi n^2}{M}\right\} \exp\left\{j\frac{2\pi mn}{M}\right\} \exp\left\{j\frac{2\pi p}{D}\right\} \\ &= u[n] \exp\left\{j\frac{2\pi mn}{M}\right\} \exp\left\{j\frac{2\pi p}{D}\right\}, \end{aligned} \tag{3}$$

where $\exp\{j\frac{2\pi mn}{M}\}$ and $\exp\{j\frac{2\pi p}{D}\}$ are the information bearing elements, i.e., FS and PS, respectively. D is the PSK modulation order and $p \in \{0, 1, \ldots, D-1\}$ is the corresponding mapping symbol. Therefore, we have $N_F = \log_2 M = SF$ and $N_P = \log_2 D$ in the conventional PSK-LoRa modulation. As a result, a total of $SF + \log_2 D$ information bits can be transmitted within each modulation symbol. In particular, the transmitted information bits are split into two sets. The first N_F bits $\{b_i\}_{i=0}^{N_F-1}$ are encoded in the FS and the last N_P bits $\{q_i\}_{i=0}^{N_P-1}$ are encoded in the PS. Therefore, the symbol mapping rules can be expressed as

$$m = \sum_{i=0}^{N_F-1} b_i 2^i, \tag{4}$$

$$p = \sum_{i=0}^{N_P-1} q_i 2^i. \tag{5}$$

As for our proposed SSK PSK-LoRa modulation, a set of M orthogonal downchirps are used along with the original upchirps and a total of $N_C + N_F + N_P$ bits can be transmitted within each modulation symbol, where $N_C = 1$, $N_F = SF$, and $N_P = \log_2 D$.[1] As shown in Fig. 1, the transmitted information bits are split into three sets, i.e., c_0, $\{b_i\}_{i=0}^{N_F-1}$, and $\{q_i\}_{i=0}^{N_P-1}$, which are encoded in the chirp rate, FS, and PS, respectively. Specifically, when $c_0 = 0$, the transmitted signal is given by

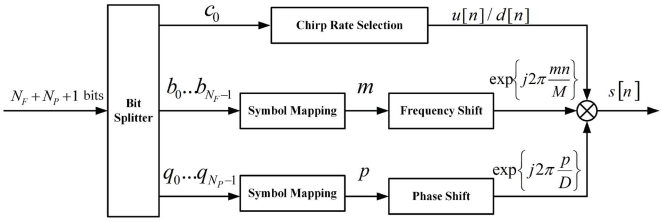

FIGURE 1. Transmitter architecture of the proposed SSK PSK-LoRa modulation.

$$s[n] = u[n] \exp\left\{j\frac{2\pi mn}{M}\right\} \exp\left\{j\frac{2\pi p}{D}\right\}, \tag{6}$$

which is identical to the conventional PSK-LoRa modulation. When $c_0 = 1$, the transmitted signal is given by

$$s[n] = d[n] \exp\left\{j\frac{2\pi mn}{M}\right\} \exp\left\{j\frac{2\pi p}{D}\right\}. \tag{7}$$

C. COHERENT DETECTION

In this section, the optimal coherent detection for the proposed SSK PSK-LoRa modulation is derived based on the maximum likelihood (ML) criterion. Assuming ideal synchronization, the received signal in AWGN channel can be expressed as

$$r[n] = s[n] + w[n], \tag{8}$$

where $w[n]$ is the additive white Gaussian noise with zero mean and variance σ^2. For simplicity, we denote $\boldsymbol{r} = [r[0], \ldots, r[M-1]]$ and $\boldsymbol{s} = [s[0], \ldots, s[M-1]]$. Hence, the likelihood function can be given as

$$\begin{aligned} p(\boldsymbol{r}|\boldsymbol{s}) &= \left(\frac{1}{\pi\sigma^2}\right)^M \exp\left\{-\frac{||\boldsymbol{r}-\boldsymbol{s}||^2}{\sigma^2}\right\} \\ &= C \exp\left\{\frac{2\Re\left\{\sum_{n=0}^{M-1} r[n]s^*[n]\right\}}{\sigma^2}\right\}, \end{aligned} \tag{9}$$

where $(\cdot)^*$ and $\Re\{\cdot\}$ denote the complex conjugate and real part extraction operators, respectively, and

$$C = \left(\frac{1}{\pi\sigma^2}\right)^M \exp\left\{-\frac{||\boldsymbol{r}||^2 + ||\boldsymbol{s}||^2}{\sigma^2}\right\}. \tag{10}$$

Note that C is independent of the mapping symbols, the ML detection can be simplified as

$$\hat{c}_0, \hat{m}, \hat{p} = \arg\max_{c_0,m,p} \Re\left\{\sum_{n=0}^{M-1} r[n]s^*[n]\right\}. \tag{11}$$

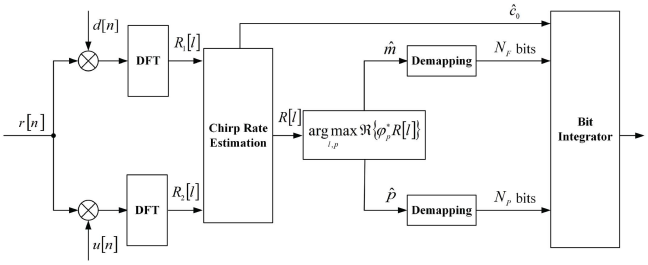

FIGURE 2. Coherent detection for SSK PSK-LoRa modulation.

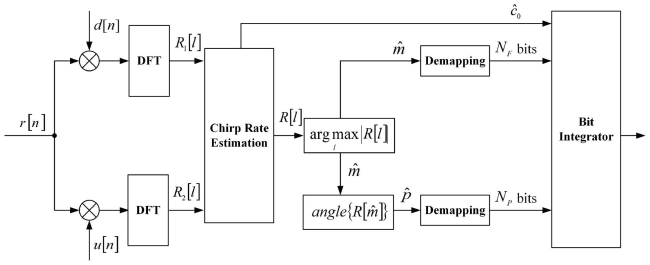

FIGURE 3. Semi-coherent detection for SSK PSK-LoRa modulation.

When $c_0 = 0$, we have

$$\begin{aligned}\sum_{n=0}^{M-1} r[n]s^*[n] &= \sum_{n=0}^{M-1} r[n]d[n]\exp\left\{-j\frac{2\pi mn}{M}\right\}\varphi_p^* \\ &= \varphi_p^* \sum_{n=0}^{M-1} r_1[n]\exp\left\{-j\frac{2\pi mn}{M}\right\} \\ &= \varphi_p^* R_1[l], \end{aligned} \tag{12}$$

where $\varphi_p = \exp\{j\frac{2\pi p}{D}\}$, $r_1[n] = r[n]d[n]$ and $R_1[l]$, $l = 0, 1, \ldots, M-1$, is the M-point DFT of $r_1[n]$. Therefore, the ML detection of the mapping symbols can be further simplified as

$$\hat{m_1}, \hat{p_1} = \arg\max_{l,p} \Re\left\{\varphi_p^* R_1[l]\right\}. \tag{13}$$

Likewise, when $c_0 = 1$, we have

$$\begin{aligned}\sum_{n=0}^{M-1} r[n]s^*[n] &= \sum_{n=0}^{M-1} r[n]u[n]\exp\left\{-j\frac{2\pi mn}{M}\right\}\varphi_p^* \\ &= \varphi_p^* \sum_{n=0}^{M-1} r_2[n]\exp\left\{-j\frac{2\pi mn}{M}\right\} \\ &= \varphi_p^* R_2[l], \end{aligned} \tag{14}$$

where $r_2[n] = r[n]u[n]$ and $R_2[l]$, $l = 0, 1, \ldots, M-1$, is the M-point DFT of $r_2[n]$. As such, the ML detection can be simplified as

$$\hat{m_2}, \hat{p_2} = \arg\max_{l,p} \Re\left\{\varphi_p^* R_2[l]\right\}. \tag{15}$$

Therefore, as shown in Fig. 2, the estimated mapping symbols can be obtained as follows. First, define $\kappa_1 = \max \Re\{\varphi_p^* R_1[l]\}$ and $\kappa_2 = \max \Re\{\varphi_p^* R_2[l]\}$. Then, using κ_1 and κ_2, the chirp rate estimation block determines $\hat{c}_0$ and $R[l]$ as

$$\hat{c}_0 = \begin{cases} 0, & \text{if } \kappa_1 > \kappa_2 \\ 1, & \text{otherwise.} \end{cases} \tag{16}$$

$$R[l] = \begin{cases} R_1[l], & \text{if } \kappa_1 > \kappa_2 \\ R_2[l], & \text{otherwise.} \end{cases} \tag{17}$$

1. The proposed SSK PSK-LoRa modulation can be easily extended to DCRK PSK-LoRa modulation where multiple discrete chirp rates are used to encode the information bits. Considering the number of available chirp rates is M_C, the number of information bits that can be carried by the chirp rate becomes $N_C = \log_2 M_C$.

Subsequently, the FS and PS mapping symbols can be jointly estimated as

$$\hat{m}, \hat{p} = \arg\max_{l,p} \Re\left\{\varphi_p^* R[l]\right\}. \tag{18}$$

Finally, the information bits encoded in the FS and PS can be recovered from the estimated symbols $\hat{m}, \hat{p}$.

D. SEMI-COHERENT DETECTION

Notably, since the initial PS of the transmitted chirp is exploited to encode the information bits, it is impossible to design a non-coherent detector for the proposed SSK PSK-LoRa modulation. In this context, both coherent and semi-coherent detection are available. Unlike coherent detection, the identification of FS and PS mapping symbols is separated in semi-coherent detection. More specifically, the FS symbol estimation is performed through non-coherent detection while the PS symbol estimation is performed via coherent detection. The corresponding receiver architecture is depicted in Fig. 3.

Firstly, the received signal $r[n]$ is multiplied by both a basic upchirp and a basic downchirp to obtain the dechirped signal $r_1[n] = r[n]d[n]$ and $r_2[n] = r[n]u[n]$. Then, $R_1[l]$ and $R_2[l]$ are obtained by taking M-point DFT of the dechirped signal $r_1[n]$ and $r_2[n]$, respectively. Define $\xi_1 = \max\{|R_1[l]|\}$ and $\xi_2 = \max\{|R_2[l]|\}$ for $l \in \{0, 1, \ldots, M-1\}$, $\hat{c}_0$ and $R[l]$ can be obtained as follows

$$\hat{c}_0 = \begin{cases} 0, & \text{if } \xi_1 > \xi_2 \\ 1, & \text{otherwise.} \end{cases} \tag{19}$$

$$R[l] = \begin{cases} R_1[l], & \text{if } \xi_1 > \xi_2 \\ R_2[l], & \text{otherwise.} \end{cases} \tag{20}$$

Then, the FS mapping symbol is given by

$$\hat{m} = \arg\max_{l} \{|R[l]|\}. \tag{21}$$

Once the estimated symbol $\hat{m}$ is obtained, the PS mapping symbol can be determined by applying the D-ary PSK demodulator, which can be expressed as

$$\hat{\varphi}_p = angle\left\{R\left[\hat{m}\right]\right\} = 2\pi\frac{\hat{p}}{D}. \tag{22}$$

Therefore, the estimated symbol $\hat{p}$ that corresponds to the PS is determined by identifying the phase of the DFT bin which has the highest peak, where $angle\{\cdot\}$ represents

TABLE 2. Time complexity of coherent and semi-coherent symbol detection.

Symbol Detection	Dechirp	DFT	FS and PS Estimation
Coherent	$\mathcal{O}(M)$	$\mathcal{O}(M\log_2 M)$	$\mathcal{O}\left(2^{N_P}M\right)$
Semi-coherent	$\mathcal{O}(M)$	$\mathcal{O}(M\log_2 M)$	$\mathcal{O}\left(M+2^{N_P}\right)$

the phase discriminator. As a result, the correct detection of FS mapping symbol is a prerequisite to the recovery of PS mapping symbol. Moreover, the PS symbol estimation is based on coherent detection under phase synchronization, i.e., the phase rotation introduced by the channel and hardware impairments is compensated, where the influence of phase offset will be discussed in Section V.

E. COMPUTATIONAL COMPLEXITY

To analyze the computational complexity of our proposed scheme, the symbol detection is divided into three stages: dechirp, DFT, FS and PS estimation. Table 2 presents a detailed time complexity analysis of both coherent and semi-coherent detection. It can be observed that the dechirp and DFT operations have the similar complexity for both coherent and semi-coherent detection. However, the joint FS and PS estimation in coherent detection results in a considerable complexity compared to the separate FS and PS estimation in semi-coherent detection. Consequently, although both coherent and semi-coherent detection require accurate phase synchronization, the former may not be feasible for many resource-constrained IoT devices [19], [20]. Therefore, semi-coherent detection is considered in the sequel due to its practical value.

III. ORTHOGONALITY AND INTERFERENCE ANALYSIS

A. ORTHOGONALITY ANALYSIS

To analyze the orthogonality of SSK PSK-LoRa symbols, we consider the inner product of two distinct symbols, i.e., $\boldsymbol{s} = [s[0], \ldots, s[M-1]]$ and $\widetilde{\boldsymbol{s}} = [\widetilde{s}[0], \ldots, \widetilde{s}[M-1]]$ as $\langle \boldsymbol{s}, \widetilde{\boldsymbol{s}} \rangle = \sum_{n=0}^{M-1} s[n]\widetilde{s}^*[n]$, where $\langle \cdot, \cdot \rangle$ represents the inner product operation. Note that the FS and PS mapping symbols are m, p in $s[n]$ and $\widetilde{m}, \widetilde{p}$ in $\widetilde{s}[n]$, respectively, and $m \neq \widetilde{m}$.

Specifically, four different cases should be evaluated: (i) both $s[n]$ and $\widetilde{s}[n]$ are generated using a basic upchirp; (ii) both $s[n]$ and $\widetilde{s}[n]$ are generated using a basic downchirp; (iii) $s[n]$ is generated using a basic upchirp while $\widetilde{s}[n]$ is generated using a basic downchirp; (iv) $s[n]$ is generated using a basic downchirp while $\widetilde{s}[n]$ is generated using a basic upchirp.

Case I: In this case, the inner product $\langle \boldsymbol{s}, \widetilde{\boldsymbol{s}} \rangle$ is given as

$$\sum_{n=0}^{M-1} s[n]\widetilde{s}^*[n] = \frac{1}{M}\varphi_p\varphi_{\widetilde{p}}^* \sum_{n=0}^{M-1} \exp\left\{j\frac{2\pi}{M}n(m-\widetilde{m})\right\} = \varphi_p\varphi_{\widetilde{p}}^*\delta[m-\widetilde{m}], \tag{23}$$

where $\varphi_p = \exp\{j\frac{2\pi p}{D}\}$, $\varphi_{\widetilde{p}} = \exp\{j\frac{2\pi\widetilde{p}}{D}\}$, and $\delta[\cdot]$ is the Kronecker delta function. Consequently, for $m \neq \widetilde{m}$, we have $\langle \boldsymbol{s}, \widetilde{\boldsymbol{s}} \rangle = 0$ in this case.

Case II: In this case, the inner product $\langle \boldsymbol{s}, \widetilde{\boldsymbol{s}} \rangle$ is given as

$$\sum_{n=0}^{M-1} s[n]\widetilde{s}^*[n] = \frac{1}{M}\varphi_p\varphi_{\widetilde{p}}^* \sum_{n=0}^{M-1} \exp\left\{j\frac{2\pi}{M}n(m-\widetilde{m})\right\} = \varphi_p\varphi_{\widetilde{p}}^*\delta[m-\widetilde{m}]. \tag{24}$$

Similarly, for $m \neq \widetilde{m}$, we also have $\langle \boldsymbol{s}, \widetilde{\boldsymbol{s}} \rangle = 0$.

Case III: The inner product $\langle \boldsymbol{s}, \widetilde{\boldsymbol{s}} \rangle$ in this case is given as

$$\begin{aligned}\sum_{n=0}^{M-1} s[n]\widetilde{s}^*[n] &= \sum_{n=0}^{M-1} u^2[n]\exp\left\{j\frac{2\pi}{M}n(m-\widetilde{m})\right\}\varphi_p\varphi_{\widetilde{p}}^* \\ &= \varphi_p\varphi_{\widetilde{p}}^* \sum_{n=0}^{M-1} u^2[n]\exp\left\{j\frac{2\pi}{M}n(m-\widetilde{m})\right\} \\ &= \frac{\varphi_p\varphi_{\widetilde{p}}^*}{M} \sum_{n=0}^{M-1} \exp\left\{j\frac{\pi}{M}\left[2n^2+2n(m-\widetilde{m})\right]\right\} \\ &= \frac{\varphi_p\varphi_{\widetilde{p}}^*}{M} I_1,\end{aligned} \tag{25}$$

where $I_1 = \sum_{n=0}^{M-1} \exp\{j\frac{\pi}{M}[2n^2 + 2n(m-\widetilde{m})]\}$ takes the form of generalized quadratic Gauss sum and its closed-form expression can be obtained according to Lemma 1.

Lemma 1: The generalized quadratic Gauss sum is given by

$$G(a,b,c) = \sum_{n=0}^{|c|-1} \exp\left\{j\frac{\pi}{c}\left(an^2+bn\right)\right\}, \tag{26}$$

where a, b, c are integers with $ac \neq 0$ and $ac + b$ is even. According to the reciprocity theorem for Gauss sums [25], we have

$$G(a,b,c) = \sqrt{|\frac{c}{a}|}\exp\left\{j\frac{\pi}{4ac}\left(|ac|-b^2\right)\right\} \sum_{n=0}^{|a|-1} \exp\left\{-j\frac{\pi}{a}\left(bn+cn^2\right)\right\}. \tag{27}$$

Therefore, we have $a = 2$, $b = 2(m-\widetilde{m})$, $c = M$ and I_1 can be computed as

$$\begin{aligned} I_1 &= \sum_{n=0}^{M-1} \exp\left\{j\frac{\pi}{M}\left[2n^2+2n(m-\widetilde{m})\right]\right\} \\ &= \sqrt{\frac{M}{2}}\exp\left\{j\frac{\pi}{8M}\left[2M-4(m-\widetilde{m})^2\right]\right\}\alpha_1, \end{aligned} \tag{28}$$

where

$$\begin{aligned}\alpha_1 &= \sum_{n=0}^{1}\exp\left\{-j\frac{\pi}{2}\left[Mn^2+2(m-\widetilde{m})n\right]\right\}\\ &= 1+\exp\left\{-j\frac{M}{2}\pi\right\}\exp\{-j\pi(m-\widetilde{m})\}\\ &= 1+\exp\{-j\pi(m-\widetilde{m})\},\end{aligned} \tag{29}$$

where the last equality holds due to the fact that $M = 2^{SF}$ with SF ranging from 7 to 12.

Therefore, if $m-\widetilde{m}$ is odd, then $\alpha_1 = 0$, which leads to $I_1 = 0$ and $\langle \boldsymbol{s}, \widetilde{\boldsymbol{s}}\rangle = 0$; if $m-\widetilde{m}$ is even, then $\alpha_1 = 2$ and I_1 can be further simplified as

$$\begin{aligned}I_1 &= 2\sqrt{\frac{M}{2}}\exp\left\{j\frac{\pi}{8M}\left[2M-4(m-\widetilde{m})^2\right]\right\}\\ &= 2\sqrt{\frac{M}{2}}\exp\left\{j\frac{\pi}{4}\right\}\exp\left\{-j\frac{\pi}{2M}(m-\widetilde{m})^2\right\}\\ &= 2\sqrt{\frac{M}{2}}\beta_1,\end{aligned} \tag{30}$$

where $\beta_1 = \exp\{j\frac{\pi}{4}\}\exp\{-j\frac{\pi}{2M}(m-\widetilde{m})^2\}$.

As a result, the inner product $\langle \boldsymbol{s}, \widetilde{\boldsymbol{s}}\rangle$ can be evaluated as

$$\left\langle \boldsymbol{s}, \widetilde{\boldsymbol{s}}\right\rangle = \begin{cases} 0, & \text{if } m-\widetilde{m} \text{ is odd}\\ \sqrt{\frac{2}{M}}\varphi_p\varphi_{\widetilde{p}}^*\beta_1, & \text{if } m-\widetilde{m} \text{ is even,}\end{cases} \tag{31}$$

which indicates the loss of orthogonality in this case.

Case IV: The inner product $\langle \boldsymbol{s}, \widetilde{\boldsymbol{s}}\rangle$ in this case is given as

$$\begin{aligned}\sum_{n=0}^{M-1} s[n]\widetilde{s}^*[n] &= \sum_{n=0}^{M-1} d^2[n]\exp\left\{j\frac{2\pi}{M}n(m-\widetilde{m})\right\}\varphi_p\varphi_{\widetilde{p}}^*\\ &= \varphi_p\varphi_{\widetilde{p}}^*\sum_{n=0}^{M-1} d^2[n]\exp\left\{j\frac{2\pi}{M}n(m-\widetilde{m})\right\}\\ &= \frac{\varphi_p\varphi_{\widetilde{p}}^*}{M}\sum_{n=0}^{M-1}\exp\left\{j\frac{\pi}{M}\left[2n(m-\widetilde{m})-2n^2\right]\right\}\\ &= \frac{\varphi_p\varphi_{\widetilde{p}}^*}{M}I_2,\end{aligned} \tag{32}$$

where I_2 also takes the form of generalized quadratic Gauss sum.

According to Lemma 1, I_2 can be computed as

$$\begin{aligned}I_2 &= \sum_{n=0}^{M-1}\exp\left\{j\frac{\pi}{M}\left[2n(m-\widetilde{m})-2n^2\right]\right\}\\ &= \sqrt{\frac{M}{2}}\exp\left\{-j\frac{\pi}{8M}\left[2M-4(m-\widetilde{m})^2\right]\right\}\alpha_2,\end{aligned} \tag{33}$$

where

$$\begin{aligned}\alpha_2 &= \sum_{n=0}^{1}\exp\left\{j\frac{\pi}{2}\left[Mn^2+2(m-\widetilde{m})n\right]\right\}\\ &= 1+\exp\left\{j\frac{M}{2}\pi\right\}\exp\{j\pi(m-\widetilde{m})\}\\ &= 1+\exp\{j\pi(m-\widetilde{m})\}.\end{aligned} \tag{34}$$

Likewise, when $m-\widetilde{m}$ is odd, $I_2 = 0$; when $m-\widetilde{m}$ is even, I_2 is obtained as

$$\begin{aligned}I_2 &= 2\sqrt{\frac{M}{2}}\exp\left\{-j\frac{\pi}{8M}\left[2M-4(m-\widetilde{m})^2\right]\right\}\\ &= 2\sqrt{\frac{M}{2}}\exp\left\{-j\frac{\pi}{4}\right\}\exp\left\{j\frac{\pi}{2M}(m-\widetilde{m})^2\right\}\\ &= 2\sqrt{\frac{M}{2}}\beta_2,\end{aligned} \tag{35}$$

where $\beta_2 = \exp\{-j\frac{\pi}{4}\}\exp\{j\frac{\pi}{2M}(m-\widetilde{m})^2\}$.

Therefore, the inner product $\langle \boldsymbol{s}, \widetilde{\boldsymbol{s}}\rangle$ in this case can be formulated as

$$\left\langle \boldsymbol{s}, \widetilde{\boldsymbol{s}}\right\rangle = \begin{cases} 0, & \text{if } m-\widetilde{m} \text{ is odd}\\ \sqrt{\frac{2}{M}}\varphi_p\varphi_{\widetilde{p}}^*\beta_2, & \text{if } m-\widetilde{m} \text{ is even,}\end{cases} \tag{36}$$

which also implies the loss of orthogonality.

Remark 1: When the two distinct symbols, i.e., $\boldsymbol{s} = [s[0], \ldots, s[M-1]]$ and $\widetilde{\boldsymbol{s}} = [\widetilde{s}[0], \ldots, \widetilde{s}[M-1]]$, are generated with the same chirp rate, they are always orthogonal and the PSs of different symbols do not impact the orthogonality. However, when $\boldsymbol{s}$ and $\widetilde{\boldsymbol{s}}$ are generated with different chirp rates, they are not always orthogonal, thus inducing interference during the detection process.

B. INTERFERENCE ANALYSIS

Relying on the above orthogonality analysis, the interference terms can be quantitatively described for the following two cases: (i) the transmitted signal is generated using a basic upchirp; (ii) the transmitted signal is generated using a basic downchirp.

Case I: In this case, the dechirped signal $r_1[n]$ is given as

$$\begin{aligned}r_1[n] &= (s[n]+w[n])d[n]\\ &= \frac{1}{M}\exp\left\{j\frac{2\pi mn}{M}\right\}\exp\left\{j\frac{2\pi p}{D}\right\}+\bar{w}[n],\end{aligned} \tag{37}$$

where $\bar{w}[n] = w[n]d[n]$ is the additive white Gaussian noise with zero mean and variance $\frac{\sigma^2}{M}$. Taking M-point DFT of $r_1[n]$, $R_1[l]$ can be obtained as

$$\begin{aligned}R_1[l] &= \sum_{n=0}^{M-1} r_1[n]\exp\left\{-j\frac{2\pi ln}{M}\right\}\\ &= \frac{\varphi_p}{M}\sum_{n=0}^{M-1}\exp\left\{j\frac{2\pi}{M}n(m-l)\right\}+\bar{W}[l]\\ &= \begin{cases}\varphi_p+\bar{W}[m], & \text{if } l=m\\ \bar{W}[l], & \text{otherwise,}\end{cases}\end{aligned} \tag{38}$$

where $\bar{W}[l] = \sum_{n=0}^{M-1}\bar{w}[n]\exp\{-j\frac{2\pi ln}{M}\}$ is the DFT of $\bar{w}[n]$ and $\bar{W}[l] \sim \mathcal{CN}(0, \sigma^2)$.

In addition, the dechirped signal $r_2[n]$ is given as

$$\begin{aligned}r_2[n] &= (s[n]+w[n])u[n]\\ &= u^2[n]\exp\left\{j\frac{2\pi mn}{M}\right\}\exp\left\{j\frac{2\pi p}{D}\right\}+\dot{w}[n],\end{aligned} \tag{39}$$

where $\dot{w}[n] = w[n]u[n] \sim \mathcal{CN}(0, \frac{\sigma^2}{M})$. Then, $R_2[l]$ can be obtained as

$$R_2[l] = \sum_{n=0}^{M-1} r_2[n] \exp\left\{-j\frac{2\pi ln}{M}\right\} = \frac{\varphi_p}{M} \sum_{n=0}^{M-1} \exp\left\{j\frac{\pi}{M}\left[2n^2 + 2n(m-l)\right]\right\} + \dot{W}[l], \quad (40)$$

where $\dot{W}[l] = \sum_{n=0}^{M-1} \dot{w}[n] \exp\{-j\frac{2\pi ln}{M}\} \sim \mathcal{CN}(0, \sigma^2)$.

According to the analysis in Section III-A, $R_2[l]$ can be further simplified as

$$R_2[l] = \begin{cases} \sqrt{\frac{2}{M}}\psi_1 + \dot{W}[l], & \text{if } m-l \text{ is even} \\ \dot{W}[l], & \text{if } m-l \text{ is odd,} \end{cases} \quad (41)$$

where $\psi_1 = \varphi_p \exp\{j\frac{\pi}{4}\} \exp\{-j\frac{\pi}{2M}(m-l)^2\}$.

According to (38) and (41), the signal-to-interference ratio (SIR) of semi-coherent detection can be given as

$$\gamma_1 = \frac{\mathbb{E}\left[|\varphi_p|^2\right]}{\mathbb{E}\left[|\sqrt{\frac{2}{M}}\psi_1|^2\right]} = \frac{M}{2}. \quad (42)$$

Consequently, the SIR can be improved with the increase of M, which implies a better performance for larger SF.

Case II: In this case, the dechirped signal $r_1[n]$ and $r_2[n]$ are given as

$$r_1[n] = (s[n] + w[n])d[n] = d^2[n] \exp\left\{j\frac{2\pi mn}{M}\right\} \exp\left\{j\frac{2\pi p}{D}\right\} + \bar{w}[n], \quad (43)$$

$$r_2[n] = (s[n] + w[n])u[n] = \frac{1}{M} \exp\left\{j\frac{2\pi mn}{M}\right\} \exp\left\{j\frac{2\pi p}{D}\right\} + \dot{w}[n]. \quad (44)$$

Likewise, $R_1[l]$ and $R_2[l]$ can be obtained as

$$R_1[l] = \sum_{n=0}^{M-1} r_1[n] \exp\left\{-j\frac{2\pi ln}{M}\right\} = \frac{\varphi_p}{M} \sum_{n=0}^{M-1} \exp\left\{j\frac{\pi}{M}\left[2n(m-l) - 2n^2\right]\right\} + \bar{W}[l], \quad (45)$$

$$R_2[l] = \sum_{n=0}^{M-1} r_2[n] \exp\left\{-j\frac{2\pi ln}{M}\right\} = \frac{\varphi_p}{M} \sum_{n=0}^{M-1} \exp\left\{j\frac{2\pi}{M}n(m-l)\right\} + \dot{W}[l]. \quad (46)$$

According to the analysis in Section III-A, $R_1[l]$ and $R_2[l]$ can be simplified as

$$R_1[l] = \begin{cases} \sqrt{\frac{2}{M}}\psi_2 + \bar{W}[l], & \text{if } m-l \text{ is even} \\ \bar{W}[l], & \text{if } m-l \text{ is odd,} \end{cases} \quad (47)$$

$$R_2[l] = \begin{cases} \varphi_p + \dot{W}[m], & \text{if } l = m \\ \dot{W}[l], & \text{otherwise,} \end{cases} \quad (48)$$

where $\psi_2 = \varphi_p \exp\{-j\frac{\pi}{4}\} \exp\{j\frac{\pi}{2M}(m-l)^2\}$. Hence, the SIR can be obtained as

$$\gamma_2 = \frac{\mathbb{E}\left[|\varphi_p|^2\right]}{\mathbb{E}\left[|\sqrt{\frac{2}{M}}\psi_2|^2\right]} = \frac{M}{2}, \quad (49)$$

which is identical to *Case I*.

IV. BER PERFORMANCE ANALYSIS

In this section, we theoretically derive the closed-form approximations for BER of the proposed scheme in both AWGN and Rayleigh fading channels. Since the interference term is proportional to $\sqrt{\frac{2}{M}}$, the proposed scheme is asymptotically orthogonal as M tends to infinity (e.g., $\sqrt{\frac{2}{M}} \leq 0.25$ for $M \geq 32$).[2] Therefore, the BER of the proposed scheme can be well approximated by the theoretical BER of an orthogonal modulation. In fact, the performance gap between the accurate and approximate BER will get negligible for large M.

A. CLOSED-FORM APPROXIMATION OVER AWGN CHANNEL

Considering the non-coherent detection of FS mapping symbol, the error performance approaches that of $2M$-ary orthogonal modulation. Consequently, the approximation of its symbol error rate (SER) over an AWGN channel can be given by[26]

$$P_{S_F}^{AWGN} = \sum_{k=1}^{2M-1} \frac{(-1)^{k+1}}{k+1} \binom{2M-1}{k} \exp\left\{-\frac{k}{k+1}\gamma_s\right\}, \quad (50)$$

where $\gamma_s = M\gamma$ is the effective SNR with γ denoting the received SNR.

Since the combination term $\binom{2M-1}{k}$ in (50) would suffer from precision problems given large values of M, a closed-form approximation for the $P_{S_F}^{AWGN}$ is given by [13]

$$P_{S_F}^{AWGN} \approx Q\left(\frac{\sqrt{\gamma_s} - \left((H_{2M-1})^2 - \frac{\pi^2}{12}\right)^{\frac{1}{4}}}{\sqrt{H_{2M-1} - \left((H_{2M-1})^2 - \frac{\pi^2}{12}\right)^{\frac{1}{2}} + 0.5}}\right), \quad (51)$$

where $Q(x) = \frac{1}{\sqrt{2\pi}} \int_x^\infty \exp(-\frac{u^2}{2})du$ and $H_N = \sum_{i=1}^{N} \frac{1}{i}$ is the Nth harmonic number.

Besides, the SER of PS mapping symbol can be well approximated by [27]

$$P_{S_P}^{AWGN} \approx 2Q\left(\sqrt{2\gamma_s}\sin\left(\frac{\pi}{D}\right)\right). \quad (52)$$

2. Note that $M = 128$ (i.e., $SF = 7$) has the worst BER performance. For larger values of M, the BER performance would get better in a similar trend.

Therefore, the closed-form BER approximation of SSK PSK-LoRa modulation over AWGN channel can be formulated as

$$P_b^{AWGN} \approx \frac{1}{2}P_{S_F}^{AWGN} + \left(1 - P_{S_F}^{AWGN}\right) \times \frac{1}{N_F + N_P + 1}P_{S_P}^{AWGN}. \quad (53)$$

The first term in (53) indicates that whenever the FS symbol estimation is wrong, a decoding error will occur on half of the total transmitted bits regardless of the correctness of PS symbol estimation. The second term, however, indicates that under the correct decision of FS mapping symbol, a decoding error will occur on only one of the total transmitted bits, which originates from the wrong estimation of PS mapping symbol considering Gray mapping.

B. CLOSED-FORM APPROXIMATION OVER RAYLEIGH FADING CHANNEL

The received signal in a frequency-flat fading channel can be expressed as

$$r[n] = hs[n] + w[n] = \sqrt{\lambda}\exp(j\theta)s[n] + w[n], \quad (54)$$

where $h = \sqrt{\lambda}\exp(j\theta)$ represents the complex channel gain ($\sqrt{\lambda}$ and θ are the channel's magnitude and phase rotation, respectively). For a Rayleigh fading channel, $\sqrt{\lambda}$ follows the Rayleigh distribution with average channel gain of 1, whereas θ is uniformly distributed over $[0, 2\pi]$.

Assuming the channel's phase rotation can be compensated at the receiver, (54) can be further simplified as

$$r[n] = \sqrt{\lambda}s[n] + w[n]. \quad (55)$$

Considering the non-coherent detection of FS mapping symbol over a Rayleigh fading channel, the approximation of its SER is also given by that of $2M$-ary orthogonal modulation [26]

$$P_{S_F}^{Ray} = \sum_{k=1}^{2M-1}(-1)^{k+1}\binom{2M-1}{k}\frac{1}{1+(k+1)\gamma_s}. \quad (56)$$

Likewise, a closed-form approximation for the SER in (56) has been given by [13]

$$P_{S_F}^{Ray} \approx Q\left(-\sqrt{2H_{2M-1}}\right) - \sqrt{\frac{\gamma_s}{\gamma_s+1}}\exp\left(-\frac{H_{2M-1}}{\gamma_s+1}\right) \times Q\left(-\sqrt{\frac{2H_{2M-1}\gamma_s}{\gamma_s+1}}\right). \quad (57)$$

Moreover, the approximate SER of PS mapping symbol over a Rayleigh fading channel is given by [27]

$$P_{S_P}^{Ray} \approx 1 - \sqrt{\frac{\gamma_s}{\gamma_s\sin^2\left(\frac{\pi}{D}\right)+1}}\sin\left(\frac{\pi}{D}\right). \quad (58)$$

Similar to (53), the closed-form BER approximation of SSK PSK-LoRa modulation over Rayleigh fading channel can be formulated as

$$P_b^{Ray} \approx \frac{1}{2}P_{S_F}^{Ray} + \frac{1}{N_F + N_P + 1}\left(1 - P_{S_F}^{Ray}\right)P_{S_P}^{Ray}. \quad (59)$$

V. NUMERICAL RESULTS AND DISCUSSION

In this section, numerical results are presented to verify the superiority of our proposed SSK PSK-LoRa modulation scheme. First, the optimal variant of the proposed scheme is determined in terms of EE. Then, we consider LoRa, E-LoRa, ICS-LoRa (interleaved-chirp-spreading LoRa) [28], SSK-LoRa, SSK ICS-LoRa [29], DCRK-CSS, and PSK-LoRa as benchmarks for comparison. The performance of these modulation schemes is evaluated in terms of: (i) BER and throughput in AWGN channel; (ii) BER and throughput in Rayleigh fading channel; (iii) BER performance in frequency-selective fading channel; (iv) BER performance under phase synchronization offset.

Remark 2: The CSS-based LoRa-like modulation schemes can be classified into three categories: (i) single chirp, (ii) multiple chirps, and (iii) multiple chirps with index modulation (IM) [30]. Compared to multi-chirp modulation, single-chirp modulation schemes usually possess a constant envelope property, which is one of the most critical aspects of low-cost implementation of IoT devices, such as the utilization of non-linear power amplifiers. As a result, single-chirp modulation schemes are more attractive in practice. Since the proposed SSK PSK-LoRa modulation belongs to single chirp modulation, we only consider the classical single chirp modulation schemes for fair comparison.

A. DETERMINATION OF OPTIMAL VARIANT

Without loss of generality, the EE can be defined as the required SNR or E_b/N_0 for correct detection at a given BER level. Herein, Fig. 4 depicts the BER performance for different variants of SSK PSK-LoRa modulation over AWGN channel. Notably, the approximate BER curves are obtained using (53).

Firstly, it can be observed that the approximate BER curves match well with the simulation results especially in the high SNR region, which validates the accuracy of our theoretical analysis in Section IV. In particular, the performance gap between the numerical and approximate curves becomes even negligible for large SF. Moreover, we can observe that both SSK BPSK-LoRa and SSK QPSK-LoRa present a slight performance loss compared to the conventional LoRa modulation. However, with the increase of PSK modulation order, a significant performance loss occurs. In particular, for a target BER of 10^{-5}, there is around 2.5 dB performance loss for SSK 8PSK-LoRa modulation, which could result in a considerable EE deterioration. Therefore, both SSK BPSK-LoRa and SSK QPSK-LoRa are the optimal variants of the proposed modulation scheme in terms of EE. Nonetheless, since one more information bit can be transmitted within each modulation symbol in SSK QPSK-LoRa modulation,

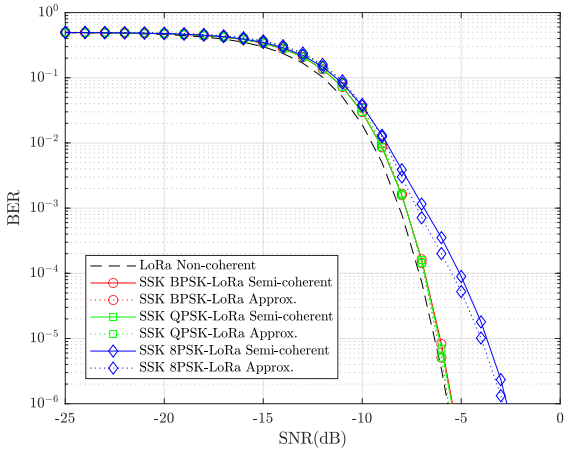

(a) $SF = 7$

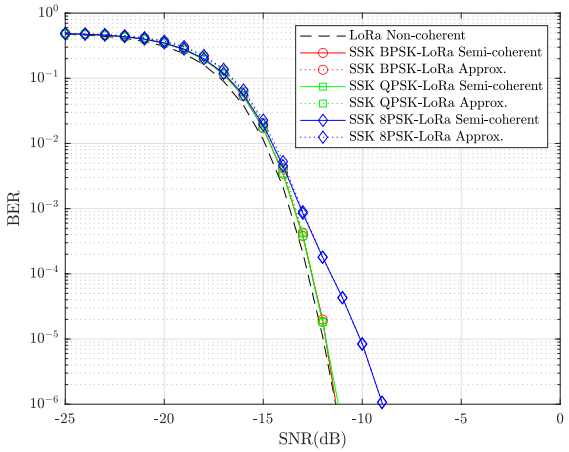

(b) $SF = 9$

FIGURE 4. BER performance for different variants of SSK PSK-LoRa modulation over AWGN channel.

it can be argued that SSK QPSK-LoRa is the optimal variant of the proposed scheme. Besides, QPSK-LoRa has also been identified as the optimal variant of the conventional PSK-LoRa modulation [19], [20]. Therefore, we only consider these optimal variants in the following performance comparison.

B. BER AND THROUGHPUT COMPARISON

In this section, we present the BER and throughput comparison of different modulation schemes. Table 3 summarizes the SE of the aforementioned modulation schemes, where N_b and η represent the number of information bits within each modulation symbol and the corresponding SE, respectively. It can be observed that the proposed SSK QPSK-LoRa modulation transmits the maximum number of information bits per symbol among these single chirp modulation schemes. Moreover, the effective throughput ρ (bps) can be calculated as

$$\rho = \eta B(1 - BER). \tag{60}$$

To illustrate the advantages of our proposed scheme more intuitively, Fig. 5 plots the BER and throughput curves

TABLE 3. The SE of the considered single chirp modulation schemes.

Modulation	N_b	η
LoRa	SF	$\frac{SF}{2^{SF}}$
E-LoRa	$SF+1$	$\frac{SF+1}{2^{SF}}$
ICS-LoRa	$SF+1$	$\frac{SF+1}{2^{SF}}$
SSK-LoRa	$SF+1$	$\frac{SF+1}{2^{SF}}$
SSK ICS-LoRa	$SF+2$	$\frac{SF+2}{2^{SF}}$
DCRK-CSS ($N_c = 2$)	$SF+2$	$\frac{SF+2}{2^{SF}}$
QPSK-LoRa	$SF+2$	$\frac{SF+2}{2^{SF}}$
SSK QPSK-LoRa	$SF+3$	$\frac{SF+3}{2^{SF}}$

versus E_b/N_0 concerning $SF = 7$ for different modulation schemes in AWGN channels. It is evident that the BER performance of our proposed SSK QPSK-LoRa is better than that of LoRa, ICS-LoRa, SSK-LoRa, SSK ICS-LoRa, and DCRK-CSS. Specifically, for a target BER of 10^{-5}, the performance gain of SSK QPSK-LoRa is around 1.3 dB for LoRa, 1.2 dB for ICS-LoRa, 1 dB for SSK-LoRa, 0.8 dB for SSK ICS-LoRa, and 0.6 dB for DCRK-CSS. Meanwhile, it also has around 0.2 dB and 0.1 dB performance gain over E-LoRa and QPSK-LoRa, respectively. The results show that the proposed modulation scheme requires lower E_b/N_0 for correct demodulation, which implies a higher EE relative to the other modulation schemes. Moreover, it can be observed that the proposed SSK QPSK-LoRa modulation provides a significant throughput improvement over other classical counterparts. Specifically, when $SF = 7$, the transmission throughput of SSK QPSK-LoRa increases by about 43% compared to the conventional LoRa modulation. Moreover, the transmission throughput improvement achieved by SSK QPSK-LoRa is about 11% compared to QPSK-LoRa, SSK ICS-LoRa, DCRK-CSS ($N_c = 2$) and 25% compared to E-LoRa, ICS-LoRa, SSK-LoRa, which demonstrates that the proposed modulation scheme outperforms the conventional LoRa and other classical counterparts in both EE and SE.

In addition, Fig. 6 illustrates that SSK QPSK-LoRa modulation exhibits a similar BER performance with E-LoRa and QPSK-LoRa in Rayleigh fading channels. However, it achieves about 1 dB performance gain compared to LoRa, ICS-LoRa, SSK-LoRa, SSK ICS-LoRa, and DCRK-CSS.

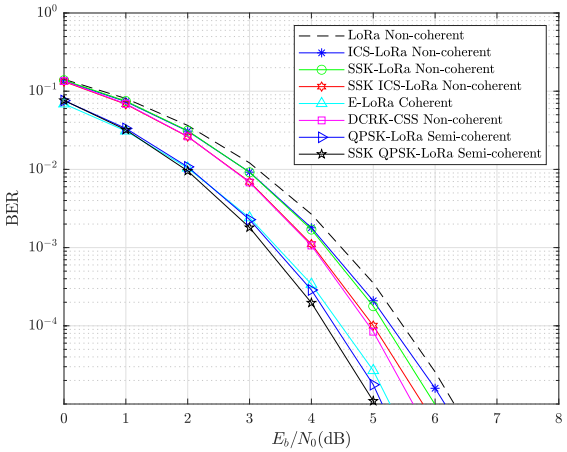

(a) BER

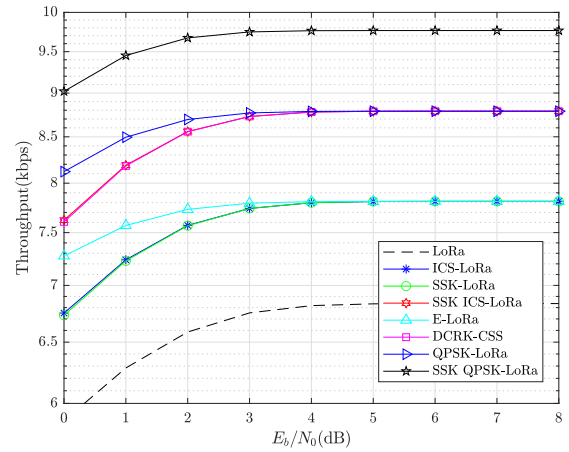

(b) Effective throughput

FIGURE 5. BER and effective throughput of different modulation schemes for $SF = 7$ and $B = 125$ kHz in AWGN channels.

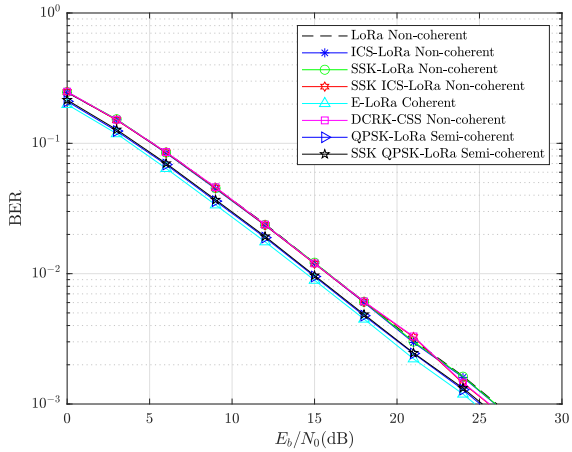

(a) BER

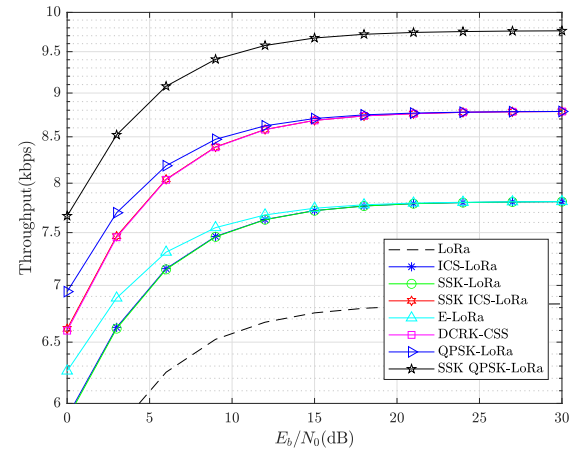

(b) Effective throughput

FIGURE 6. BER and effective throughput of different modulation schemes for $SF = 7$ and $B = 125$ kHz in Rayleigh fading channels.

This is mainly due to the fact that the PS mapping symbol is less sensitive to channel fading than the FS mapping symbol. Moreover, the Rayleigh fading imposes a considerable impact on the BER performance, which boils down to the degradation of EE and effective throughput. To deal with the severe performance loss in Rayleigh fading channels, the robustness of communication can be enhanced by using suitable Forward Error Correction (FEC) strategies. The current LoRa PHY layer adopts Hamming code as its FEC strategy, which has been widely investigated in the literature [31], [32], [33]. Alternative channel coding solutions, such as Turbo code [34] and LDPC (low-density parity-check) code [35], have been further studied in LoRa-based communication systems. Moreover, other relevant techniques, such as MIMO-LoRa (multiple-input-multiple-output LoRa) [36], [37] and RIS (reconfigurable intelligent surface) assisted LoRa [38], have also been proposed, which can effectively reduce the impact of fading channels. Nonetheless, research on more advanced solutions to achieve better BER performance is still of great significance.

C. BER PERFORMANCE IN FREQUENCY-SELECTIVE FADING CHANNELS

In this section, we consider the BER performance in a frequency-selective fading channel with impulse response $h[n] = \sqrt{0.8}\delta[n] + \sqrt{0.2}\delta[n-1]$, like that in [11]. It can be seen from Fig. 7 that for a target BER of 10^{-5}, the proposed SSK QPSK-LoRa modulation presents a performance loss of around 3.5 dB compared to Fig. 5(a). Nonetheless, it still achieves the best BER performance relative to the other classical counterparts.

D. BER PERFORMANCE UNDER PHASE SYNCHRONIZATION ERRORS

In this section, we analyze the BER performance under phase synchronization errors which are expected to exist in practical wireless communications. The received signal with phase synchronization errors can be given as

$$r[n] = s[n]\exp\{j\theta\} + w[n], \tag{61}$$

where θ denotes the phase offset (PO).

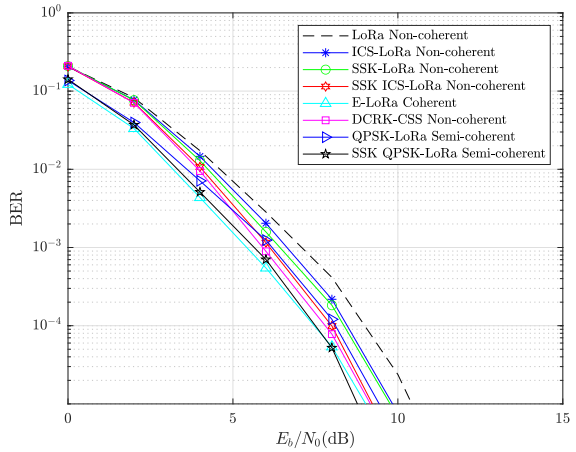

FIGURE 7. BER performance of different modulation schemes for $SF = 7$ in frequency-selective fading channels.

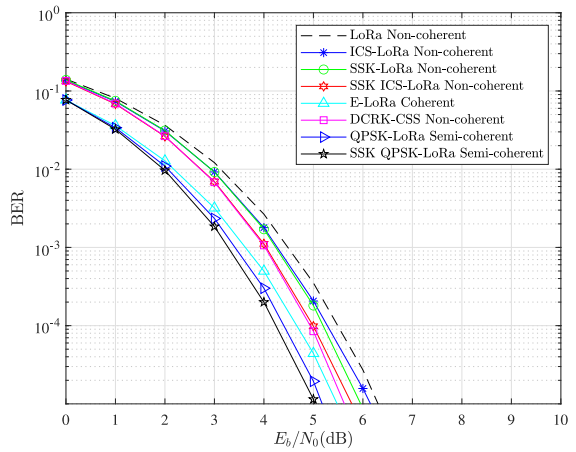

(a) $\theta = \pi/16$

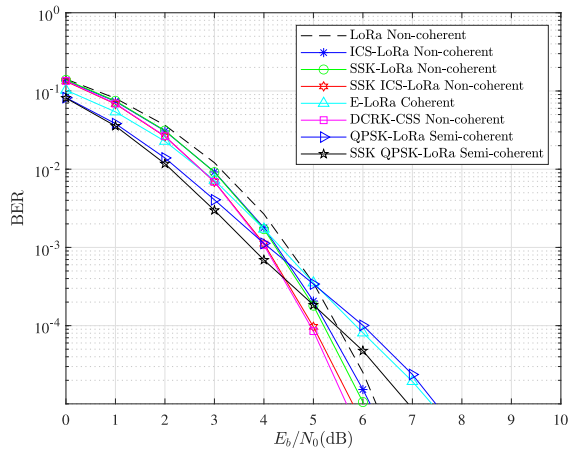

(b) $\theta = \pi/8$

FIGURE 8. BER performance of different modulation schemes for $SF = 7$ with PO in AWGN channels.

Fig. 8 depicts the BER performance of different modulation schemes with PO. Although the initial PSs are utilized to carry the information bits, both QPSK-LoRa and SSK QPSK-LoRa are robust to small PO. Compared to Fig. 5(a), it can be observed that when $\theta = \pi/16$, the performance loss of the proposed scheme is negligible compared to when $\theta = 0$. In this case, the proposed SSK QPSK-LoRa still exhibits the best performance among these single chirp modulation schemes. However, the BER performance deteriorates as the PO increases. It can be observed that when $\theta = \pi/8$, the performance loss of the proposed scheme is about 2 dB at the BER level of 10^{-5}, which cannot be ignored. By contrast, benefited from the non-coherent detection, the BER performance of LoRa, ICS-LoRa, SSK-LoRa, SSK ICS-LoRa, and DCRK-CSS is not affected by the PO.

VI. CONCLUSION

In this paper, we have proposed SSK PSK-LoRa modulation as an extension of the existing multi-parameter CSS modulation schemes. The transceiver architecture of the proposed scheme has been presented along with both coherent and semi-coherent detection methods. Moreover, based on the orthogonality and interference analysis, an overall performance evaluation of the proposed scheme has been provided. Both analytical and numerical results demonstrate that the proposed scheme outperforms most classical counterparts in terms of energy and spectral efficiency, making it a promising candidate for heterogeneous application domains in the future 6G enabled high-data-rate IoT era.

REFERENCES

[1] F. Guo, F. R. Yu, H. Zhang, X. Li, H. Ji, and V. C. M. Leung, "Enabling massive IoT toward 6G: A comprehensive survey," *IEEE Internet Things J.*, vol. 8, no. 15, pp. 11891–11915, Aug. 2021.

[2] R. Liu, R. Y.-N. Li, M. D. Renzo, and L. Hanzo, "A vision and an evolutionary framework for 6G: Scenarios, capabilities and enablers," 2023, *arXiv:2305.13887*.

[3] A. Zaidi, Y. Hussain, M. Hogan, and C. Kuhlins, "Cellular IoT evolution for industry digitalization," Ericsson, Stockholm, Sweden, White Paper GFMC-19, 2019.

[4] D. C. Nguyen et al., "6G Internet of Things: A comprehensive survey," *IEEE Internet Things J.*, vol. 9, no. 1, pp. 359–383, Jan. 2022.

[5] U. Raza, P. Kulkarni, and M. Sooriyabandara, "Low power wide area networks: An overview," *IEEE Commun. Surveys Tuts.*, vol. 19, no. 2, pp. 855–873, 2nd Quart., 2017.

[6] Y. Chen, Y. A. Sambo, O. Onireti, and M. A. Imran, "A survey on LPWAN-5G integration: Main challenges and potential solutions," *IEEE Access*, vol. 10, pp. 32132–32149, 2022.

[7] C. Milarokostas, D. Tsolkas, N. Passas, and L. Merakos, "A comprehensive study on LPWANs with a focus on the potential of LoRa/LoRaWAN systems," *IEEE Commun. Surveys Tuts.*, vol. 25, no. 1, pp. 825–867, 1st Quart., 2023.

[8] P. Gkotsiopoulos, D. Zorbas, and C. Douligeris, "Performance determinants in LoRa networks: A literature review," *IEEE Commun. Surveys Tuts.*, vol. 23, no. 3, pp. 1721–1758, 3rd Quart., 2021.

[9] M. Vaezi et al., "Cellular, wide-area, and non-terrestrial IoT: A survey on 5G advances and the road toward 6G," *IEEE Commun. Surveys Tuts.*, vol. 24, no. 2, pp. 1117–1174, 2nd Quart., 2022.

[10] H. Jradi, F. Nouvel, A. E. Samhat, J.-C. Prévotet, and M. Mroue, "A seamless integration solution for LoRaWAN into 5G system," *IEEE Internet Things J.*, early access, Apr. 17, 2023, doi: 10.1109/JIOT.2023.3267502.

[11] L. Vangelista, "Frequency shift chirp modulation: The LoRa modulation," *IEEE Signal Process. Lett.*, vol. 24, no. 12, pp. 1818–1821, Dec. 2017.

[12] M. Chiani and A. Elzanaty, "On the LoRa modulation for IoT: Waveform properties and spectral analysis," *IEEE Internet Things J.*, vol. 6, no. 5, pp. 8463–8470, Oct. 2019.

[13] T. Elshabrawy and J. Robert, "Closed-form approximation of LoRa modulation BER performance," *IEEE Commun. Lett.*, vol. 22, no. 9, pp. 1778–1781, Sep. 2018.
[14] F. Adelantado, X. Vilajosana, P. Tuset-Peiro, B. Martinez, J. Melia-Segui, and T. Watteyne, "Understanding the limits of LoRaWAN," *IEEE Commun. Mag.*, vol. 55, no. 9, pp. 34–40, Sep. 2017.
[15] W. Xu et al., "The design, implementation, and deployment of a smart lighting system for smart buildings," *IEEE Internet Things J.*, vol. 6, no. 4, pp. 7266–7281, Aug. 2019.
[16] A. Staikopoulos, V. Kanakaris, and G. A. Papakostas, "Image transmission via LoRa networks—A survey," in *Proc. IEEE Int. Conf. Image Vis. Comput.*, Beijing, China, 2020, pp. 150–154.
[17] D. Magrin, M. Capuzzo, A. Zanella, L. Vangelista, and M. Zorzi, "Performance analysis of LoRaWAN in industrial scenarios," *IEEE Trans. Ind. Informat.*, vol. 17, no. 9, pp. 6241–6250, Sep. 2021.
[18] H. H. R. Sherazi, L. A. Grieco, M. A. Imran, and G. Boggia, "Energy-efficient LoRaWAN for industry 4.0 applications," *IEEE Trans. Ind. Informat.*, vol. 17, no. 2, pp. 891–902, Feb. 2021.
[19] T. T. Nguyen, H. H. Nguyen, R. Barton, and P. Grossetete, "Efficient design of chirp spread spectrum modulation for low-power wide-area networks," *IEEE Internet Things J.*, vol. 6, no. 6, pp. 9503–9515, Dec. 2019.
[20] R. Bomfin, M. Chafii, and G. Fettweis, "A novel modulation for IoT: PSK-LoRa," in *Proc. IEEE Veh. Technol. Conf.*, Apr. 2019, pp. 1–5.
[21] T. Elshabrawy, P. Edward, M. Ashour, and J. Robert, "On the different mathematical realizations for the digital synthesis of LoRa-based modulation," in *Proc. 25th Eur. Wireless Conf.*, 2019, pp. 1–6.
[22] A. W. Azim, J. L. G. Monsalve, and M. Chafii, "Enhanced PSK-LoRa," *IEEE Wireless Commun. Lett.*, vol. 11, no. 3, pp. 612–616, Mar. 2022.
[23] M. Hanif and H. H. Nguyen, "Slope-shift keying LoRa-based modulation," *IEEE Internet Things J.*, vol. 8, no. 1, pp. 211–221, Jan. 2021.
[24] I. B. F. de Almeida, M. Chafii, A. Nimr, and G. Fettweis, "Alternative chirp spread spectrum techniques for LPWANs," *IEEE Trans. Green Commun. Netw.*, vol. 5, no. 4, pp. 1846–1855, Dec. 2021.
[25] B. C. Berndt, K. S. Williams, and R. J. Evans, *Gauss and Jacobi Sums*. New York, NY, USA: Wiley, 1998.
[26] M. K. Simon and M.-S. Alouini, *Digital Communication Over Fading Channels*, 2nd ed. Hoboken, NJ, USA: Wiley, 2005.
[27] A. Goldsmith, *Wireless Communications*. Cambridge, U.K.: Cambridge Univ. Press, 2005.
[28] T. Elshabrawy and J. Robert, "Interleaved chirp spreading LoRa-based modulation," *IEEE Internet Things J.*, vol. 6, no. 2, pp. 3855–3863, Apr. 2019.
[29] A. Mondal, M. Hanif, and H. H. Nguyen, "SSK-ICS LoRa: A LoRa-based modulation scheme with constant envelope and enhanced data rate," *IEEE Commun. Lett.*, vol. 26, no. 5, pp. 1185–1189, May 2022.
[30] A. W. Azim, A. Bazzi, R. Shubair, and M. Chafii, "Chirp spread spectrum-based waveform design and detection mechanisms for LPWAN-based IoT—A survey," 2022, *arXiv:2208.10274*.
[31] G. Baruffa, L. Rugini, V. Mecarelli, L. Germani, and F. Frescura, "Coded LoRa performance in wireless channels," in *Proc. IEEE Annu. Int. Symp. Pers. Indoor Mobile Radio Commun. (PIMRC)*, Sep. 2019, pp. 1–6.
[32] T. Elshabrawy and J. Robert, "Evaluation of the BER performance of LoRa communication using BICM decoding," in *Proc. IEEE 9th Int. Conf. Consum. Electron. (ICCE-Berlin)*, Sep. 2019, pp. 162–167.
[33] O. Afisiadis, A. Burg, and A. Balatsoukas-Stimming, "Coded LoRa frame error rate analysis," in *Proc. IEEE Int. Conf. Commun. (ICC)*, Jun. 2020, pp. 1–6.
[34] S. An, Z. Lu, H. Wang, and Q. Yu, "A turbo coded LoRa-index modulation scheme for IoT communication," in *Proc. IEEE 21st Int. Conf. Commun. Technol.*, Tianjin, China, 2021, pp. 736–740.
[35] J. Bourduge, C. Poulliat, B. Gadat, and J. F. Chouteau, "Bit interleaved chirp spread spectrum coded modulations with iterative decoding based on LDPC codes for coherent and non-coherent regimes," in *Proc. IEEE 33rd Annu. Int. Symp. Pers. Indoor Mobile Radio Commun. (PIMRC)*, Kyoto, Japan, 2022, pp. 968–974.
[36] H. Ma, G. Cai, Y. Fang, P. Chen, and G. Han, "Design and performance analysis of a new STBC-MIMO LoRa system," *IEEE Trans. Commun.*, vol. 69, no. 9, pp. 5744–5757, Sep. 2021.
[37] T. K. Nguyen, H. H. Nguyen, and E. Bedeer, "Performance improvement of LoRa modulation with signal combining and semi-coherent detection," *IEEE Commun. Lett.*, vol. 25, no. 9, pp. 2889–2893, Sep. 2021.
[38] X. Zhang, W. Xu, G. Cai, Y. Song, and G. Chen, "A new reconfigurable intelligent-surface-assisted LoRa system," *IEEE Trans. Veh. Technol.*, vol. 71, no. 8, pp. 9055–9060, Aug. 2022.

QUANTAO YU received the B.S. degree from the Beijing Institute of Technology, China, in 2020, where he is currently pursuing the Ph.D. degree in information and communication systems. His current research interests include LoRa, Internet of Things, and spread-spectrum modulation.

DONGXUAN HE received the B.S. degree in automation and Ph.D. degree in information and communication systems from the Beijing Institute of Technology (BIT) in 2013 and 2019, respectively. He was a visiting student with the Singapore University of Technology and Design from 2017 to 2018 and a Postdoctoral Researcher with the Department of Electronic Engineering, Tsinghua University from 2019 to 2022. He is currently an Assistant Professor with the School of Information and Electronics, BIT. His current research interests include terahertz communication, AI empowered wireless communications, and physical layer security. He was also an Exemplary Reviewer of IEEE WIRELESS COMMUNICATIONS LETTERS.

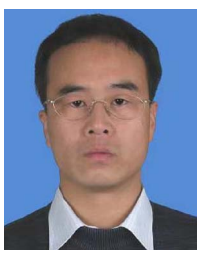

ZHIPING LU received the M.S. degree in computer science from the University of Chinese Academy of Science in 2008. He is currently pursuing the Ph.D. degree in information and communication engineering from the Beijing University of Posts and Telecommunications and also with the State Key Laboratory of Wireless Mobile Communications, China Academy of Telecommunications Technology. His research interests include wireless communications and artificial intelligence.

HUA WANG (Member, IEEE) received the Ph.D. degree from the Beijing Institute of Technology, Beijing, China, in 1999, where he is currently a Professor with School of Information and Electronics. From February 2009 to January 2010, he was a Visiting Professor with the Department of Electrical Engineering, Arizona State University, USA. His research interests are in the fields of communication theory and signal processing, wireless networking, modem design, and implementation for satellite communication.